

PACS numbers: 42.25.Dd; 42.25.Fx; 42.30.Wb
DOI: 10.1070/QE2006v036n11ABEH013302

Time-domain diffuse optical tomography using analytic statistical characteristics of photon trajectories

A.B. Konovalov, V.V. Vlasov, A.G. Kalintsev, O.V. Kravtsenyuk, V.V. Lyubimov

***Abstract*. The inverse problem of diffuse optical tomography (DOT) is reduced by the method of photon average trajectories (PAT) to the solution of the integral equation integrated along the conditional mean statistical photon trajectory. The PAT bending near the flat boundary of a scattering medium is estimated analytically. These estimates are used to determine the analytic statistical characteristics of photon trajectories for the flat layer geometry. The inverse DOT problem is solved by using the multiplicative algebraic algorithm modified to improve the convergence of the iteration reconstruction process. The numerical experiment shows that the modified PAT method permits the reconstruction of near-surface optical inhomogeneities virtually without distortions.**

Keywords: *diffuse optical tomography, method of photon average trajectories, multiplicative algebraic reconstruction technique, spatially variant blurring model.*

1. Introduction

Like projection tomography (X-ray computed, single-photon emission computed, positron emission), the diffuse optical tomography (DOT) of a strongly scattering medium initially poses a forward problem, i.e. the problem of propagation of radiation through a medium and then formulates and solves the inverse problem of the reconstruction of spatial distributions of optical parameters of the medium. The main problem of DOT is multiple light scattering which produces the diffusion of photons and excludes the presence of any regular photon trajectories. Because of this, the forward problem is solved by using the exact models of light propagation through matter: the radiation transfer equation [1 – 4], its diffusion approximation [1, 5 – 8] or the Monte-Carlo method [9 – 11]. The analytic solutions of the radiation transfer equation for the flat layer geometry studied in our paper were analysed by Kokhanovsky [2, 3]. The solutions of the diffusion equation for the same geometry were obtained by many authors, for example, by Arridge et al. [7] and Contini et al. [8]. When a flat layer is a random medium, the radiation transfer (or diffusion) equation is solved numerically by the method of finite elements [5, 6] or finite differences [4]. The inverse DOT problem is strongly nonlinear due to the nonlinear dependence of the photon flux on optical parameters (absorption and scattering coefficients, the refractive index) being reconstructed. For this reason, the direct use of standard algorithms of projection tomography [12 – 14] based on the linear Radon transformation causes the distortion and blurring of structures reproduces in tomograms [15, 16].

The local linearization of the inverse problem of DOT is performed, as a rule, by using multistep reconstruction techniques [4 – 6] based on the variational formulation of the equation describing the propagation of light. A typical example is the Newton – Raphson algorithm with the Levenberg – Marcuardt iteration procedure [6]. Multistep algorithms provide a relatively high spatial resolution ($\sim$5 mm) for diffusion tomograms, but they are not fast enough to perform real-time medical diagnostics because the forward problem should be solved numerically many times by adjusting at each linearization step not only the solution vector but also the matrix of coefficients of a system of algebraic equations describing the discrete model.

To accelerate the reconstruction procedure, we developed the alternative method [17 – 27] based on the probabilistic interpretation of radiation energy transfer by photons from a source to a detector. According to this method, the inverse problem of DOT is reduced to the solution of the integral equation integrated along the mean statistical photon trajectory (PAT). The use of conditional PATs makes it possible to pass from the multistep to single-step reconstruction model by employing the fast algorithms of projection tomography to reconstruct optical parameters [12 – 14]. Note that integrals along photon trajectories were studied analytically by using the radiation transfer equation in [28]. Perelman et al. [29, 30] used the probabilistic approach, which is close to that presented in this paper, to calculate integrals along average (most probable) trajectories and analyse time-resolved signals. However, the reconstruction of spatial distributions of optical parameters was not considered in these papers.

A.B. Konovalov, V.V. Vlasov E.I. Zababakhin All-Russian Research Institute of Technical Physics, Russian Federal Nuclear Centre, P.O. Box 245, Snezhinsk, Chelyabinsk region, Russia;
e-mail: a_konov2003@yahoo.com;
A.G. Kalintsev, V.V. Lyubimov Research Institute for Laser Physics, Birzhevaya lin. 16, 119034 St. Petersburg, Russia;
O.V. Kravtsenyuk Institute of Electronic Structure & Laser – Foundation for Research and Technology – Hellas (IESL-FORTH), P.O. Box 1527, Vassilika Vouton, 71110 Heraklion, Crete;
e-mail: olgakr@iesl.forth.gr

Received 16 June 2006; revision received 25 July 2006
Kvantovaya Elektronika **36** (11) 1048 – 1055 (2006)
Translated by M.N. Sapozhnikov

We have shown in our previous papers by the example of the 2D reconstruction from the data simulated for the pulsed detection scheme of time-resolved signals that the PAT method can be successfully realised by using both algebraic [22, 23, 26] and integral algorithms [24, 25, 27]. By filtrating shadows from optical inhomogeneities [24–26] or performing the spatially variant restoration of reconstructed tomograms [27], it is possible to obtain the spatial resolution no worse than the resolution of reconstructions obtained with the use of multistep algorithms. In this case, the advantage in the calculation time achieves two orders of magnitude.

So far all our realisations of the PAT method were based on the three-segment approximation of curvilinear PATs and time dependences of the velocity of centres of mass of the instant distributions of diffusion photons (so-called diffusion photon clouds). Such an approach makes it possible not only to reconstruct rapidly the image but also calculate in real time the matrix of the weight coefficients of the system of equations (when algebraic algorithms are used) before the image reconstruction. However, the three-segment approximation is correct and does not deteriorate the reconstruction quality only if optical inhomogeneities are located far enough from the boundaries of a scattering object, where PATs are close to straight lines and the velocities of the centres of mass of diffusion clouds are almost constant. Near the boundaries, where PATs bend and centres of mass are accelerated, approximation errors can cause distortions in the reconstruction of the spatial structures of optical inhomogeneities [22]. To improve the reconstruction quality of boundary inhomogeneities, we abandoned in this paper for the first time the three-segment approximation and used analytic statistical characteristics of photon trajectories in the reconstruction. These characteristics include the PAT itself, the velocity of the centre of mass of the diffusion photon cloud, and the standard root-mean-square deviation (RMSD) of the photon position from the PAT. We studied analytically variations in these characteristics near the flat surface of a scattering medium. The derived relations were used to find average trajectories and velocities corresponding to the specified set of point sources and detectors for the flat layer geometry (the 2D case was considered).

Based on the dependences obtained in the paper, a discrete reconstruction model is realised. Tomograms were reconstructed by model shadows from absorbing inhomogeneities by using the multiplicative algebraic reconstruction technique (MART) [12, 13], which we modified to improve the divergence of the iteration process. The matrix of the weight coefficients of a system of equations was constructed by considering intersections with the quantisation cells of the reconstruction region of not PATs themselves but the so-called banana-like bands whose thickness amounts to $\sim 30\,\%$ of the RMSD of photons from the PAT. During the reconstruction, the weight smoothing was performed for each of the iterations taking into account the nonuniform introduction of corrections to different quantisation cells. Tomograms reconstructed from shadows were restored by using the spatially variant image blurring model, which was described in detail in [27]. The results were visualised and compared with similar results obtained by using the three-segment approximation of the statistical characteristics of photon trajectories. It is shown that the new realisation of the PAT method considerably improves the quality of tomograms in the case of the reconstruction of inhomogeneities located near the boundaries of a scattering object.

2. Analytic statistical characteristics of photon trajectories

Let us assume that the photon density in a volume V of a scattering medium restricted by the piecewise smooth surface $\partial\Omega$ satisfies the time-dependent diffusion equation with an instant point source

$$\frac{\partial\varphi(\boldsymbol{r}_1,\tau)}{\partial\tau} - \nabla\left[D(\boldsymbol{r}_1)v(\boldsymbol{r}_1)\nabla\varphi(\boldsymbol{r}_1,\tau)\right] + \mu_{\mathrm{a}}(\boldsymbol{r}_1)v(\boldsymbol{r}_1)\varphi(\boldsymbol{r}_1,\tau) = \delta(\boldsymbol{r}_1-\boldsymbol{r}_{\mathrm{s}},\tau), \tag{1}$$

where $D(\boldsymbol{r}_1)$ is the diffusion coefficient; $\mu_{\mathrm{a}}(\boldsymbol{r}_1)$ is the absorption coefficient; $v(\boldsymbol{r}_1)=c/n(\boldsymbol{r}_1)$ is the speed of light in the medium; c is the speed of light in vacuum; $n(\boldsymbol{r}_1)$ is the refractive index; and $\delta(\boldsymbol{r}_1-\boldsymbol{r}_{\mathrm{s}},\tau)$ is the Dirac delta function. Then, the conditional probability density that a photon migrating from the spatiotemporal point $(\boldsymbol{r}_{\mathrm{s}},0)(\boldsymbol{r}_{\mathrm{s}}\in V)$ to the spatiotemporal point $(\boldsymbol{r},t)(\boldsymbol{r}\in\partial\Omega)$ will be at the instant τ at a spatial point with coordinates $\boldsymbol{r}_1\in V$ will be described by the expression

$$P(\boldsymbol{r}_1,\tau;\boldsymbol{r},t) = \frac{\varphi(\boldsymbol{r}_1,\tau)\partial G(\boldsymbol{r},t;\boldsymbol{r}_1,\tau)/\partial\eta}{\partial\varphi(\boldsymbol{r},t)/\partial\eta} \tag{2}$$

if the Dirichlet boundary condition is used and the expression

$$P(\boldsymbol{r}_1,\tau;\boldsymbol{r},t) = \frac{\varphi(\boldsymbol{r}_1,\tau)G(\boldsymbol{r},t;\boldsymbol{r}_1,\tau)}{\varphi(\boldsymbol{r},t)} \tag{3}$$

in the Robin boundary condition is used [19, 20, 22]. Here, $G(\boldsymbol{r},t;\boldsymbol{r}_1,\tau)$ is the Green function; $\partial/\partial\eta$ is the derivative along the external normal to the surface $\partial\Omega$ at the point $\boldsymbol{r}$. The conditional probability density $P(\boldsymbol{r}_1,\tau;\boldsymbol{r},t)$ as a function of the variable $\boldsymbol{r}_1$ describes at each fixed moment τ the instantaneous distributions of diffusion photons (diffusion clouds), while the time integral $\int_0^\tau P(\boldsymbol{r}_1,\xi;\boldsymbol{r},t)\mathrm{d}\xi$ describes the instantaneous distributions of trajectories of diffusion photons. At the instant $\tau=t$, this integral forms the region of the most probable photon trajectories migrating from point $(\boldsymbol{r}_{\mathrm{s}},0)$ to point $(\boldsymbol{r},t)$ (banana-like region). The function $P(\boldsymbol{r}_1,\tau;\boldsymbol{r},t)$ allows us to describe approximately this region with the help of statistical moments

$$\boldsymbol{R}(\boldsymbol{r},t,\tau) = \int_V \boldsymbol{r}_1 P(\boldsymbol{r}_1,\tau;\boldsymbol{r},t)\mathrm{d}^3 r_1, \tag{4}$$

$$\Delta(\boldsymbol{r},t,\tau) = \left[\int_V |\boldsymbol{r}_1-\boldsymbol{R}(\boldsymbol{r}_1,t,\tau)|^2 P(\boldsymbol{r}_1,\tau;\boldsymbol{r},t)\mathrm{d}^3 r_1\right]^{1/2}. \tag{5}$$

The first moment $\boldsymbol{R}(\boldsymbol{r},t,\tau)$ is the radius vector describing the movement of the centre of mass of the photon distribution from point $(\boldsymbol{r}_{\mathrm{s}},0)$ to point $(\boldsymbol{r},t)$. The trajectory of the centre of mass is in fact the PAT. The second moment $\Delta(\boldsymbol{r},t,\tau)$ describes the standard RMSD of photons from the PAT and characterises the effective width of the banana-like region at each instant of time τ. The value

$$v_{\rm cl}(\tau) = \left| \frac{{\rm d}\boldsymbol{R}(\tau)}{{\rm d}\tau} \right| = \frac{{\rm d}l(\tau)}{{\rm d}\tau}, \tag{6}$$

where $l(\tau)$ is the distance propagated along the PAT for the time τ, is the velocity of the centre of mass of the instant photon distribution propagating along the PAT (hereafter, the velocity of the diffusion cloud).

It was shown [17, 18, 20] that the centre of mass of the diffusion cloud in a homogeneous infinite medium moves from a source to a detector uniformly and linearly. The PAT bending and a change in the velocity in the absence of contrast inhomogeneities can be caused only by the closeness of the object boundary. Let us study variations in the statistical characteristics near the flat surface of a scattering medium. We assume that an instantaneous point source is located in a homogeneous half-space $z \geqslant 0$ at the point $(0, 0, z_0)$ and $z_0 \gg 1/\mu_{\rm s}'$, where $\mu_{\rm s}'$ is the reduced scattering coefficient. Consider, for example, the Dirichlet boundary condition $\varphi(\boldsymbol{r}_1, \tau)|_{z=0} = 0$. According to [17–19], the function $\varphi(\boldsymbol{r}_1, \tau)$ and the Green function $G(\boldsymbol{r}, t; \boldsymbol{r}_1, \tau)$ of the diffusion equation are described by the expressions

$$\varphi(\boldsymbol{r}_1, \tau) = \left(\frac{4\pi D_0 c\tau}{n_0} \right)^{-3/2} \exp\left(- \frac{\mu_{\rm a0} c\tau}{n_0} \right) \times \left\{ \exp\left[- \frac{x_1^2 + y_1^2 + (z_1 - z_0)^2}{4D_0 c\tau} n_0 \right] - \exp\left[- \frac{x_1^2 + y_1^2 + (z_1 + z_0)^2}{4D_0 c\tau} n_0 \right] \right\}, \tag{7}$$

$$G(\boldsymbol{r}, t; \boldsymbol{r}_1, \tau) = \left[\frac{4\pi D_0 c(t-\tau)}{n_0} \right]^{-3/2} \exp\left[- \frac{\mu_{\rm a0} c(t-\tau)}{n_0} \right] \times \left\{ \exp\left[- \frac{(x - x_1)^2 + (y - y_1)^2 + (z - z_1)^2}{4D_0 c(t-\tau)} n_0 \right] - \exp\left[- \frac{(x - x_1)^2 + (y - y_1)^2 + (z + z_1)^2}{4D_0 c(t-\tau)} n_0 \right] \right\}, \tag{8}$$

where D_0, $\mu_{\rm a0}$, and n_0 are the optical parameters of a homogeneous medium. Let us assume for simplicity of calculations that a detector is located at the point $(x_0, 0, 0)$ at the medium boundary $z = 0$. Then, taking into account that $y = 0$ and $z = 0$, we obtain

$$\left. \frac{\partial}{\partial \eta} G(\boldsymbol{r}, t; \boldsymbol{r}_1, \tau) \right|_{y=0, z=0} = \left[\frac{4\pi D_0 c(t-\tau)}{n_0} \right]^{-3/2} \times \exp\left[- \frac{\mu_{\rm a0} c(t-\tau)}{n_0} \right] \frac{z_1 n_0}{D_0 c(t-\tau)} \times \exp\left[- \frac{(x_1 - x)^2 + y_1^2 + z_1^2}{4D_0 c(t-\tau)} n_0 \right], \tag{9}$$

$$\left. \frac{\partial}{\partial \eta} \varphi(\boldsymbol{r}, t) \right|_{y=0, z=0} = \left(\frac{4\pi D_0 ct}{n_0} \right)^{-3/2} \times \exp\left(- \frac{\mu_{\rm a0} ct}{n_0} \right) \frac{z_0 n_0}{D_0 ct} \exp\left(- \frac{z_0^2 + x^2}{4D_0 ct} n_0 \right). \tag{10}$$

By substituting expressions (7), (9), and (10) into (2), we obtain

$$P(\boldsymbol{r}_1, \tau; \boldsymbol{r}, t)\Big|_{y=0, z=0} = \frac{2}{z_0} \left(\frac{4\pi D_0 c\tau}{n_0} \right)^{-3/2} \left(1 - \frac{\tau}{t} \right)^{-5/2} \times \exp\left[- \frac{z_0^2 n_0 (t-\tau)}{4D_0 ct\tau} - \frac{x^2 n_0 \tau}{4D_0 ct(t-\tau)} \right] \times \exp\left[- x_1^2 \frac{n_0 t}{4D_0 c\tau(t-\tau)} + x_1 \frac{x n_0}{2D_0 c(t-\tau)} \right] \times \exp\left[- y_1^2 \frac{n_0 t}{4D_0 c\tau(t-\tau)} \right] z_1 \sinh\left(z_1 \frac{z_0 n_0}{2D_0 c\tau} \right) \times \exp\left[- z_1^2 \frac{n_0 t}{4D_0 c\tau(t-\tau)} \right]. \tag{11}$$

By substituting (11) into (4) and integrating over the volume of the scattering medium $z \geqslant 0$, we obtain the expressions for coordinates of the centre of mass of the diffusion cloud that moves from the point $(0, 0, z_0)$ of the source to the point $(x_0, 0, 0)$ of the detector:

$$\begin{aligned} X(\tau) &= x_0 \frac{\tau}{t}, \\ Y(\tau) &= 0, \\ Z(\tau) &= z_0 \left\{ \left[1 + \frac{\tau}{t} \left(\frac{\alpha}{2} - 1 \right) \right] {\rm erf}\left(\frac{t-\tau}{\alpha\tau} \right)^{1/2} + \left[\frac{\alpha\tau(t-\tau)}{\pi t^2} \right]^{1/2} \exp\left(- \frac{t-\tau}{\alpha\tau} \right) \right\}, \end{aligned} \tag{12}$$

where $\alpha = 4D_0 ct/(z_0^2 n_0)$ and ${\rm erf}\,\xi$ is the probability integral. Correspondingly, the velocity of the diffusion cloud is

$$v_{\rm cl}(\tau) = \left[\left(\frac{{\rm d}X}{{\rm d}\tau} \right)^2 + \left(\frac{{\rm d}Y}{{\rm d}\tau} \right)^2 + \left(\frac{{\rm d}Z}{{\rm d}\tau} \right)^2 \right]^{1/2}, \tag{13}$$

where

$$\begin{aligned} \frac{{\rm d}X}{{\rm d}\tau} &= \frac{x_0}{t}; \\ \frac{{\rm d}Y}{{\rm d}\tau} &= 0; \\ \frac{{\rm d}Z}{{\rm d}\tau} &= \frac{z_0}{t} \left\{ \left(\frac{\alpha}{2} - 1 \right) {\rm erf}\left(\frac{t-\tau}{\alpha\tau} \right)^{1/2} - \left[\frac{\alpha\tau}{\pi(t-\tau)} \right]^{1/2} \times \exp\left(- \frac{t-\tau}{\alpha\tau} \right) \right\}. \end{aligned} \tag{14}$$

The aim of this paper is to study the possibility of the qualitative reconstruction of optical inhomogeneities of a scattering medium restricted by two planes. A typical example of the practical application of the flat layer geometry (the case of $d \gg 1/\mu_{\rm s}'$, where d is the layer thickness) is the diffuse optical reconstructive mammography [31–34]. A woman breast is tightly placed between two glass plates, on which radiation sources and detectors are located, thereby taking the form of a layer. It is obvious that the derivation of relations of the type (12) and (14) for

the flat layer geometry involves bulky calculations. Therefore, it is expedient to find the PAT and velocities of movement of diffusion clouds between the two planes by using analytic results obtained for the half-space.

The basic assumption in this case is that the character of PAT bending and the change in the velocity $v_{cl}(\tau)$ near the planes of the source S and detector D is the same (Fig. 1) and the influence of the opposite boundary is negligibly small [19, 20]. In this case, the centre of mass of the diffusion cloud propagates the distance SO, as the distance OD, for the time $t/2$. If the centre of mass moved in the half-space $z \geqslant 0$ from a point S_0 to the point D through the point O, it would pass the interval S_0O for the time $t/2$. Because the velocity component along the x axis is a constant, the point S_0 lies on the perpendicular to SS' to the medium boundary. The distance S_0S' can be found by solving numerically the equation $Z(\tau = t/2) = d/2$ with respect to z_0 [see relation (12)]. Then, the part OD of the trajectory can be calculated by expression (12) and the part SO can be obtained by its symmetric reflection with respect to the point O.

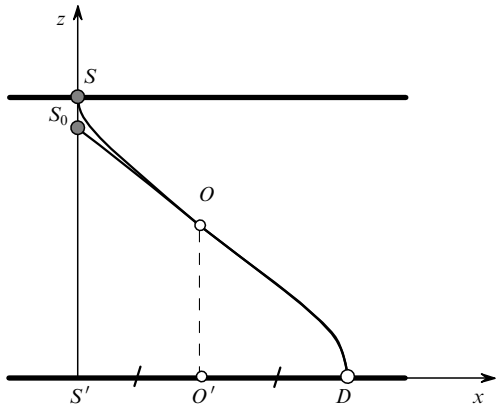

Figure 1. Construction of the PAT for the flat layer geometry.

Figure 2 presents the geometry of data detection that we selected for the case of the 2D reconstruction. Triangles and circles indicate the positions of radiation sources and detectors, respectively. As an example, Fig. 2 also shows six average trajectories constructed by using the above-described algorithm for the time $t = 3000$ ps and optical parameters $D_0 = 0.066$ cm and $n_0 = 1.4$. For comparison, the dashed curves present piecewise linear approximations of the PAT. We studied in this paper the object probing regime in transmission, i.e. only connections between radiation sources and detectors located on the opposite sides of the object were considered. The total number of average trajectories was 32×16.

3. Algorithm for solving the inverse problem

Let us define the relative shadow g of optical inhomogeneities as the logarithm of the ratio of intensities I_0 and I of the unperturbed and perturbed signals, respectively, detected on the surface $\partial\Omega$ at the instant t. We assume that the first approximation of the perturbation theory is valid ($I_0 - I \ll I_0$), and the perturbation of a signal is caused by the presence of the local change $\delta\mu_a(\boldsymbol{r}_1) = \mu_a(\boldsymbol{r}_1) - \mu_{a0}$ in the absorption coefficient μ_{a0} (without the loss of generality of the PAT method, we restrict ourselves here to the case of an absorbing inhomogeneity). Then, the inverse problem of the time-domain DOT is reduced to the solution of the integral equation [19, 21, 22]

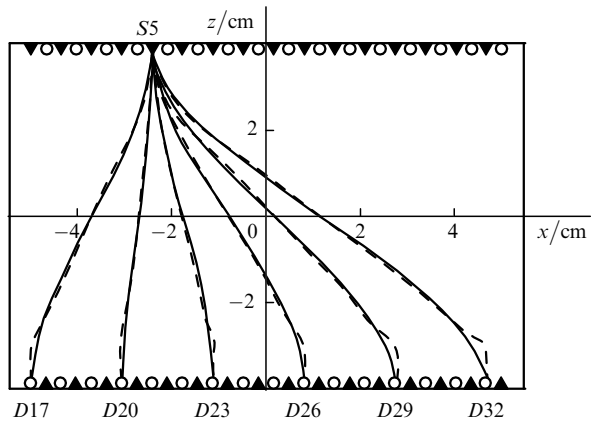

Figure 2. Geometry of the data detection for a rectangular object. Coordinates of the indicated sources and detectors (in centimetres): $S5$ – $(-2.52, 4)$, $D17$ – $(-5, -4)$, $D20$ – $(-3.06, -4)$, $D23$ – $(-1.13, -4)$, $D26$ – $(0.81, -4)$, $D29$ – $(2.74, -4)$, and $D32$ – $(4.68, -4)$.

$$g(L,t) = \int_L \frac{c}{n_0 v_{cl}(l)} \left[\int_V \delta\mu_a(\boldsymbol{r}_1) P(\boldsymbol{r}_1, \tau; \boldsymbol{r}, t) \mathrm{d}^3 r_1 \right] \mathrm{d}l, \quad (15)$$

where L is the PAT and $v_{cl}(l)$ is the velocity of the diffusion cloud as a function of $l(\tau)$. Equation (15) can be solved for the function in the brackets in the integrand, i.e. the function $\delta\mu_a(\boldsymbol{r}_1)$ averaged over the spatial distribution of photons contributing to the signal detected at the instant t. Thus, the solution of the inverse problem assumes the performance of the two successive steps: (i) the reconstruction of tomograms blurred due to averaging from a set of relative shadows and (ii) the restoration of the obtained tomograms by using a blurring model to compensate for the blurring effect.

The generalised discrete model of the 2D reconstruction problem is constructed as usual [22]. A Cartesian grid of square image elements covering an object is introduced. Let the function $\int_V \delta\mu_a(\boldsymbol{r}_1) P(\boldsymbol{r}_1, \tau; \boldsymbol{r}, t) \mathrm{d}^3 r_1$ being reconstructed have a constant value f_{kl} within the image element with the subscripts k and l [hereafter, the (k,l) cell]. Let L_{ij} be the PAT connecting the ith source with the jth detector, and g_{ij} be the relative shadow of the ith source measured with the jth detector. Then, the discrete model of the reconstruction problem can be described by the system of linear algebraic equations

$$g_{ij} = \sum_{k,l} W_{ijkl} f_{kl}, \quad (16)$$

where W_{ijkl} is the weight of the contribution of the (k,l) cell to the total change in the signal g_{ij} along the entire trajectory L_{ij}. To improve the convergence of the iteration reconstruction process compared to [22], we modified the method for calculating the matrix of the weight coefficients $\boldsymbol{W} = \{W_{ijkl}\}$ by using the approach often employed in projection geometry [35, 36]. The idea is to consider the intersection of not the PAT itself with the (k,l) cell but of a narrow band of finite thickness. In projection tomography, such bands have the form of an elongated rectangular or a

cone. In our case, it is expedient to use a banana-like band of width directly proportional to the RMSD of a photon from the PAT: $\varepsilon = \gamma\Delta(\tau)$. The high calculation accuracy of the PAT is this case is not of principal importance. Therefore, according to the conclusion [19] that the RMSD is independent in fact of the object shape, a simple expression for an infinite space can be used

$$\Delta(\tau) = \left[\frac{2D_0 c(t-\tau)\tau}{n_0 t}\right]^{1/2}. \tag{17}$$

The proportionality coefficient $\gamma \in (0,1)$ is selected to provide the complete filling of the object area by all the bands. Figure 3 shows such a filling for γ equal to 0.05 (Fig. 3a) and 0.3 (Fig. 3b) and the delay time of detectors $t = 300$ ps. Optical parameters correspond to the values presented in section 2. The delay time used in calculations corresponds to the initial part of the leading edge of the temporal point spread function in the case of oppositely located sources and detectors or to the initial part of the trailing edge when sources and detectors are most removed from each other. Figure 3a demonstrates large regions which are not intersected by bands (shown by white). This means in fact that a thickly grid will contain cells to which no correction will be introduced during the reconstruction process. These regions are negligibly small in Fig. 3b, which reduces the probability of appearance of 'dead' cells to a minimum. Because of this, we used the value $\gamma = 0.3$ in calculations.

The weight W_{ijkl} is determined from the expression

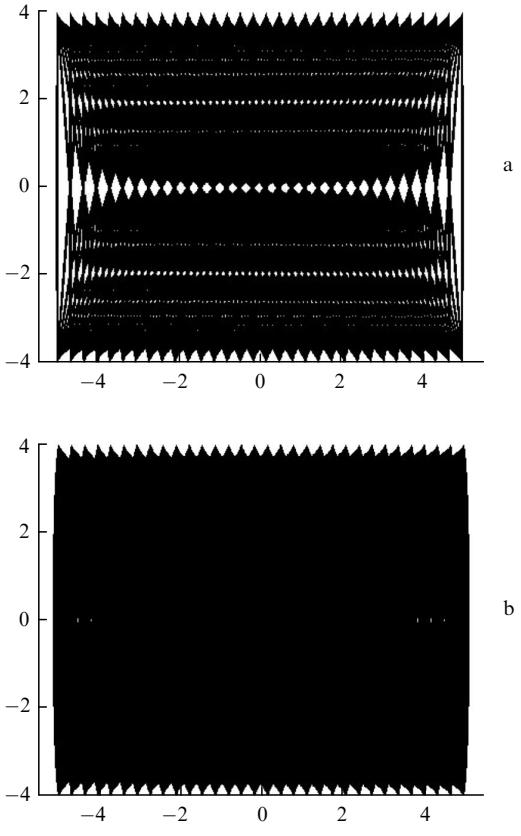

Figure 3. Regions of the object filling by banana-like bands for $\gamma = 0.05$ (a) and 0.3 (b) (axes are in centimetres).

$$W_{ijkl} = \frac{c}{n_0 v_{ijkl}^{\mathrm{cl}}}\frac{S_{ijkl}}{\delta}, \tag{18}$$

where S_{ijkl} is the intersection area of the banana-like band connecting the ith source and the jth detector [hereafter, the (i,j) band] with the (k,l) cell (Fig. 4); v_{ijkl}^{cl} is the discrete value of the velocity of the diffusion cloud calculated for the (kl) cell and (i,j) band; and δ is the cell size. The set of values $\{v_{ijkl}^{\mathrm{cl}}\}$ is found by using the following algorithm.

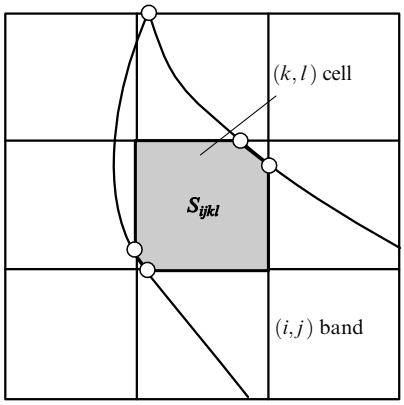

Figure 4. Intersection of the (i,j) band with the (k,l) cell.

(i) The sequence $\{\tau_p\}$ of discrete values of instants of time is specified.

(ii) Perpendiculars to the tangents of the considered trajectory L_{ij} are constructed at points corresponding to times $\{\tau_p\}$ (Fig. 5).

(iii) The cycle over p is organised in which

– the intersection cells of the (i,j) band and the band formed by two adjacent perpendiculars corresponding to the instants τ_p and τ_{p+1} are found (these cells are shown by grey in Fig. 5);

– the value of the mean velocity $[v_{\mathrm{cl}}(\tau_p) + v_{\mathrm{cl}}(\tau_{p+1})]/2$ for the two instants is written into all the cells found;

– if some value $(v_{ijkl}^{\mathrm{cl}})_{\mathrm{old}}$ was already written in a cell, the recalculation is performed by the expression

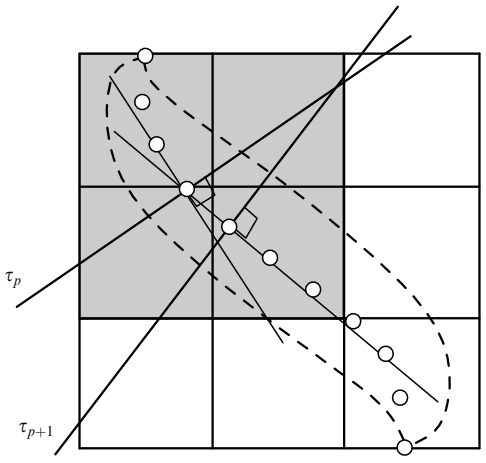

Figure 5. Scheme for determining discrete velocities of the diffusion cloud.

$$v_{ijkl}^{\mathrm{cl}} = \frac{(v_{ijkl}^{\mathrm{cl}})_{\mathrm{old}} N + (v_{ijkl}^{\mathrm{cl}})_{\mathrm{new}}}{N+1}, \tag{19}$$

where $(v_{ijkl}^{\mathrm{cl}})_{\mathrm{new}}$ is a new value and N is the number of recalculations that have been already performed.

(iv) All the PATs are successively sorted out and the procedure is repeated for each of them beginning from step (ii).

Corrections are introduced to the image being reconstructed in each $(s+1)$th iteration by using the expression

$$f_{kl}^{(s+1)} = f_{kl}^{(s)} \left(g_{ij} \Big/ \sum_{k,l} W_{ijkl} f_{kl}^{(s)} \right)^{\lambda W_{ijkl}/\tilde{W}_{kl}}, \tag{20}$$

where $\tilde{W}_{kl} = \sum_{i,j} W_{ijkl}$; $\lambda \in (0,1)$ is the parameter controlling the convergence rate of the iteration process. To improve the convergence, we performed smoothing in each of the iterations taking into account the distributions of the number of introduced corrections $\{A_{kl}\}$ and the sum of weights $\{\tilde{W}_{kl}\}$ over cells:

$$f_{kl}^{(s+1)} = \frac{1}{(2r+1)^2} \sum_{m=-r}^{r} \sum_{n=-r}^{r} f_{k+m,l+n}^{(s+1)} \tilde{W}_{k+m,l+n} A_{k+m,l+n}, \tag{21}$$

where the integer r specifies the size $(r \times r)$ of the smoothing window. Expressions (20) and (21) describing the MART modified by us take into account, unlike other realisations of this algorithm [22, 35, 36], the nonuniformity of the number of corrections introduced into different cells. Distributions $\{A_{kl}\}$ and $\{\tilde{W}_{kl}\}$ for the 100×137 net that we used for calculations are presented in Fig. 6. The iteration process is interrupted when the specified convergence rate v_{conv} is achieved

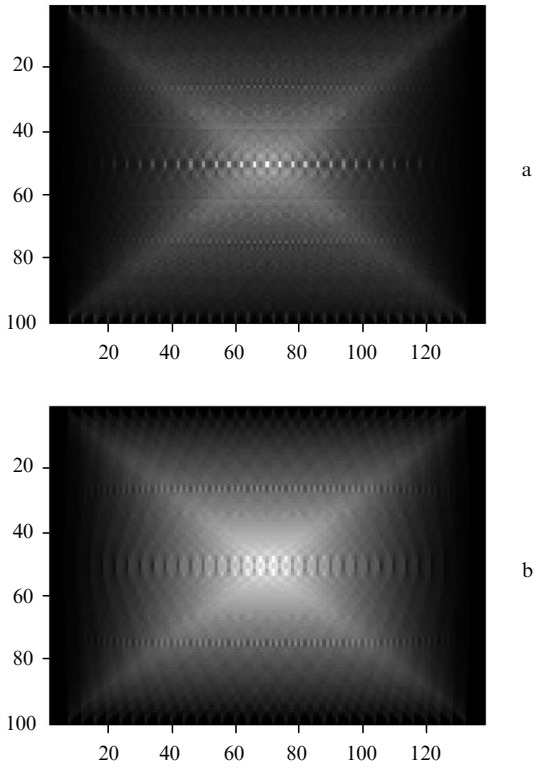

Figure 6. Distribution of the number of corrections $\{A_{kl}\}$ introduced to the reconstructed image (a) and sums of weights $\{W_{kl}\}$ (b) on the 100×137 grid.

$$\frac{\rho^{(s+1)} - \rho^{(s)}}{\rho^{(s)}} \leqslant v_{\mathrm{conv}}, \tag{22}$$

where

$$\rho^{(s)} = \sum_{i,j} \left(g_{ij} - \sum_{k,l} W_{ijkl} f_{kl}^{(s)} \right)^2.$$

The blurring of tomograms $\boldsymbol{f}$ reconstructed from shadows was compensated during using the spatially variant blurring model [37]. According to this model, the discrete restoration problem is described by the system of linear algebraic equation

$$\boldsymbol{f} = \boldsymbol{P}\boldsymbol{x}, \tag{23}$$

where $\boldsymbol{P}$ is a large ill-conditioned matrix describing the blurring operator, and $\boldsymbol{x}$ is the discrete representation of the required solution $\delta\mu_{\mathrm{a}}(\boldsymbol{r}_1)$. The model is based on the division of an image into regions, each of them being described by its own spatially invariant point spread function (PSF). These functions are interpolated and are written into the matrix $\boldsymbol{P}$ so that the matrix contains all the nonzero elements of each of the spatially invariant PSFs corresponding to separate regions of the tomogram. In addition, the matrix $\boldsymbol{P}$ takes into account *a priori* information about the extrapolation of the restored image outside boundaries, i.e. the boundary conditions. This is necessary to compensate for near-surface artefacts appearing due to the Gibbs effect. For example, in the case of the reflection boundary conditions that we used in the restoration, the matrix $\boldsymbol{P}$ is a sum of two matrices: the extended block Toeplitz matrix [38] with extended Toeplitz blocks and the extended block Hankel matrix with extended Hankel blocks [39].

Each spatially invariant PSF corresponding to a separate region of the tomogram was simulated by performing the following sequence of operations.

(i) A point inhomogeneity with the amplitude that is an order of magnitude greater than the amplitude $\delta\mu_{\mathrm{a}}(\boldsymbol{r}_1)$ is specified on a triangle grid by three values at the nodes of a triangle located at the centre of the region.

(ii) Shadows from the point inhomogeneity are simulated by solving numerically Eqn (1) by the method of finite elements.

(iii) A tomogram with the PSF is reconstructed from the obtained model shadows by using the modified MART.

The system (23) was inverted by using the iterative algorithm of steepest descent with the minimisation of the residual norm of the solution [40]. This algorithm converges rapidly enough and has a quasi-convergence with respect to the relative error $\|\boldsymbol{x}_s - \boldsymbol{x}\|/\|\boldsymbol{x}\|$, where $\boldsymbol{x}_s$ is the approximation at the sth iteration. This is important for obtaining the regularised solution. The restoration procedure of diffuse optical tomograms reconstructed by the PAT method is described in detail in [27] and is not considered here.

4. Results and discussion

To demonstrate the possibilities of the modified PAT method, we carried out the calculation experiment by specifying numerically scattering objects with absorbing

inhomogeneities, simulating the relative shadows from inhomogeneities, and performing the reconstruction and restoration procedures described in section 3. We considered two scattering rectangular objects of size 11×8 cm (Fig. 2). The refractive index, the diffusion and absorption coefficients of the objects were 1.4, 0.66 cm, and 0.05 cm^{-1}, respectively. Each of the objects contains two circular absorbing inhomogeneities of diameter 0.8 cm separated by a distance of 0.8 cm. The Cartesian coordinates of the centres of inhomogeneities in the coordinate system in Fig. 2 were (in centimetres) $(-0.8, 0)$ and $(0.8, 0)$ for the first object and $(-0.8, 3.3)$ and $(0.8, 3.3)$ for the second object. The absorption coefficient of the inhomogeneities was 0.075 cm^{-1}. The arrangement of sources and detectors is shown in Fig. 2.

Figure 7a shows inhomogeneities specified on the triangle high-resolution grid containing 13859 nodes and 7108 elements. The relative shadows from inhomogeneities were simulated by solving numerically Eqn (1) by the method of finite elements. Each object was reconstructed from model shadows on the 100×137 grid by using the modernised MART. The stabilised solution was obtained already after ten – twelve iterations. The reconstruction time per iteration was $\sim$12 s, from which 5 s were spent for introducing corrections by expression (20) and 7 – 8 s were spent for smoothing with the 3×3 window [according to (21)]. Hereafter, the calculation times are presented for programs written for MATLAB and a 1.7-GHz Pentium PC with the 256-Mb random-access memory. Figure 7b presents the results of the reconstruction of inhomogeneities of the objects.

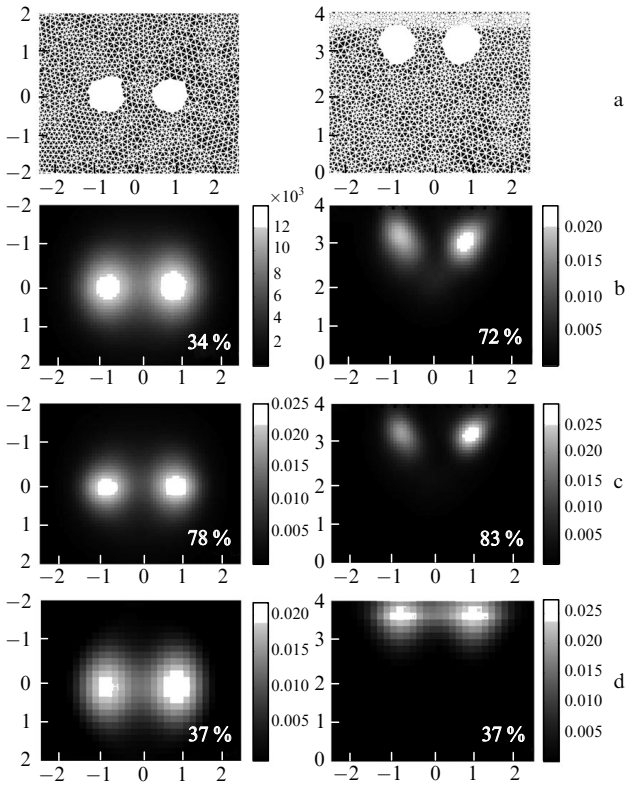

Figure 7. Results of the reconstruction and restoration of tomograms (axes are in centimetres, the palette scale is in inverse centimetres). The image regions of size 5×4 cm containing inhomogeneities are shown.

Tomograms were restored by the spatially variant method [37] by dividing the image into two regions, each of them containing its own inhomogeneity. The PSF was simulated by specifying a point inhomogeneity in a triangle at the centre of the circular inhomogeneity. A tomogram with inhomogeneities remote from boundaries was restored by performing ten iterations. In the case of near-boundary inhomogeneities, the regularised solution was obtained already after three iterations. The restoration time per iteration was 6 s. The results of the restoration are presented in Fig. 7c. Figure 7d shows the final results of the reconstruction – restoration procedure for the case of the three-segment approximation of statistical characteristics (the 50×68 grid). In this case, the reconstruction was performed by lines rather than by bands, as described above. We failed to obtain adequate results on a thickly grid because of a strong rarefaction of the matrix of weight coefficients. Note that the time of reconstruction by lines with smoothing was smaller by a factor of three than in the case of reconstruction by banana-like bands for the same number of iterations. The spatial resolution of the modified PAT method was quantitatively estimated by measuring modulation transfer coefficients from the profiles of obtained images [22, 24, 25, 27] for structures of size 0.8 cm. These estimates are presented at the right bottom corners of the corresponding images in Fig. 7.

An analysis of the results shows that structures of size 0.8 cm are reliably resolved in all tomograms presented in Fig. 7. However, in passing from the reconstruction by piecewise-linear PATs to the reconstruction by banana-like bands, we obtain more than the twofold advantage in the reproduced contrast: 78 % versus 37 % in the case of inhomogeneities remote from boundaries and 83 % versus 37 % in the case of near-boundary inhomogeneities. In the latter case, not only the spatial resolution is improved, but also structure distortions caused by the three-segment approximation are compensated to a great extent. Indeed, Fig. 7d (on the right) demonstrates the false displacement of structures to the boundary. As a result, inhomogeneities completely merge with the boundary. On the contrary, in Figs 7b and c the gap between the boundary and inhomogeneities is distinctly resolved. In this case, positions of the centres of inhomogeneities coincide with those in the initial model image. The restoration effect for near-boundary structures was small: the image contrast increased from 72 % to 83 % after restoration. This can be explained by a relatively weak blurring of structures compared to the central region. As a whole, the modified PAT method provides higher quality imaging compared to its previous realisations based on the three-segment approximation of statistical characteristics.

It follows from the data presented above that the described method is inferior in the calculation time to ultrafast line reconstruction algorithms. This is explained by a more rarefied matrix of the weight coefficients, which requires more calculations. In this paper, we did not optimise the duration of the reconstruction – restoration procedure. The aim of the paper was to demonstrate the principal outlook of the new method of calculating weight coefficients for improving the quality of tomograms. In the future, algorithms that are faster than the MART can be used to invert system (16), for example, the conjugated gradient algorithm for the least square problem [41] and the least square algorithm with the QR factorisation [42]. The

structure blurring effect can be compensated by the filtration of shadows in the frequency region instead of the time-consuming post-processing of reconstructed tomograms [26]. In addition, it is expedient to use a faster calculation medium than MATLAB. All this will reduce the time of calculations by the modified PAT method.

5. Conclusions

We have studied the principal possibility of improving the quality of diffuse optical tomograms by using the modified method of photon average trajectories with the pulsed detection scheme of a time-resolved signal. The modification consists in abandoning the piecewise-linear approximation of statistical characteristics of photon trajectories used previously and employing analytic dependences for calculations. We have refined the method for calculating the weight coefficients in the discrete reconstruction problem, which considerably improved the convergence of the multiplicative algebraic reconstruction technique used for the reconstruction of tomograms. The possibilities of the modified method of photon average trajectories have been demonstrated in the computational experiment on the 2D reconstruction of two scattering rectangular objects with absorbing inhomogeneities. It has been shown that when inhomogeneities are located near the boundary, the image quality can be considerably improved compared to the previous realisations of the method. It has been pointed out that, although the realisation of the method considered in the paper is somewhat inferior in the calculation rate to previous realisations (due to the increase in the amount of calculations), the reconstruction time can be optimised in the future.

Acknowledgements. The authors thank N.A. Shamina for her help in calculations and useful discussions. O.V. Kravtsenyuk acknowledges the support of the European Community and the 6th Program of Marie Curie for the Support of Foreign Scientists (Grant No. MIF1-CT-2005-008330).

References

1. Ishimaru A. *Wave Propagation and Scattering in Random Media* (New York: Academic Press, 1978; Moscow: Mir, 1981) Vol. 1.
2. Kokhanovsky A.A. *Meas. Sci. Technol.*, **13**, 233 (2002).
3. Kokhanovsky A.A. *Light Scattering Media Optics: Problems and Solutions* (Berlin: Springer, 2004).
4. Klose A.D., Hielscher A.H. *Med. Phys.*, **26**, 1698 (1999).
5. Yodh A., Chance B. *Phys. Today*, **48**, 34 (1995).
6. Arridge S.R. *Inverse Problems*, **15**, R41 (1999).
7. Arridge S.R., Cope M., Delpy D.T. *Phys. Med. Biol.*, **37**, 1531 (1992).
8. Contini D., Martelli F., Zaccanti G. *Appl. Opt.*, **36**, 4587 (1997).
9. Feng S., Zeng F., Chance B. *Proc. SPIE Int. Soc. Opt. Eng.*, **1888**, 78 (1993).
10. Zaccanti G. *Appl. Opt.*, **30**, 2031 (1991).
11. Martelli F., Contini D., Taddeucci A., Zaccanti G. *Appl. Opt.*, **36**, 4600 (1997).
12. Gordon R., Bender R., Herman G.T. *J. Theor. Biol.*, **29**, 471 (1970).
13. Censor Y. *Trudy IIER*, **71**, 148 (1983) [*Proc. IEEE*, **71**, 409 (1983)].
14. Lewitt R.M. *Trudy IIER*, **71**, 125 (1983) [*Proc. IEEE*, **71**, 390 (1983)].
15. Grable R.I. US Patent 5692511 (1997).
16. Colak S.B., Papaioannou D.G., Hooft W.G., van der Mark M.B., Schomberg H., Paasschens J.C.J., Melissen J.B.M., van Asten N.A.A. *J. Appl. Opt.*, **36**, 180 (1997).
17. Lyubimov V.V. *Proc. SPIE Int. Soc. Opt. Eng.*, **2769**, 107 (1995).
18. Lyubimov V.V. *Opt. Spektrosk.*, **80**, 687 (1996).
19. Volkonskii V.B., Kravtsenyuk O.V., Lyubimov V.V., Mironov E.P., Murzin A.G. *Opt. Spektrosk.*, **86**, 299 (1999).
20. Kravtsenyuk O.V., Lyubimov V.V. *Opt. Spektrosk.*, **88**, 670 (2000).
21. Kravtsenyuk O.V., Lyubimov V.V. *Opt. Spektrosk.*, **89**, 119 (2000).
22. Lyubimov V.V., Kalintsev A.G., Konovalov A.B., Lyamtsev O.V., Kravtsenyuk O.V., Murzin A.G., Golubkina O.V., Mordvinov G.B., Soms L.N., Yavorskaya L.M. *Phys. Med. Biol.*, **47**, 2109 (2002).
23. Golubkina O.V., Kalintsev A.G., Konovalov A.B., Kravtsenyuk O.V., Lyamtsev O.V., Lyubimov V.V., Mordvinov G.B., Murzin A.G., Soms L.N., Tokareva N.O., Yavorskaya L.M. *Proc. SPIE Int. Soc. Opt. Eng.*, **4431**, 275 (2001).
24. Konovalov A.B., Lyubimov V.V., Kutuzov I.I., Kravtsenyuk O.V., Murzin A.G., Mordvinov G.B., Soms L.N., Yavorskaya L.M. *J. Electron. Imaging*, **12**, 602 (2003).
25. Lyubimov V.V., Konovalov A.B., Kutuzov I.I., Kravtsenyuk O.V., Kalintsev A.G., Murzin A.G., Golubkina O.V., Soms L.N., Yavorskaya L.M. *Opt. Zh.*, **70**, 37 (2003).
26. Kalintsev A.G., Kalintseva N.A., Kravtsenyuk O.V., Lyubimov V.V. *Opt. Spektrosk.*, **99**, 162 (2005).
27. Konovalov A.B., Mogilenskikh D.V., Lyubimov V.V. *Proc. SPIE Int. Soc. Opt. Eng.*, **5859**, 585918 (2005).
28. Tessendorf J. *Phys. Rev. A*, **35**, 872 (1987).
29. Perelman L.T., Wu J., Wang Y., Itzkan I., Dasari R.R., Feld M.S. *Phys. Rev. E*, **51**, 6134 (1995).
30. Perelman L.T., Wu J., Itzkan I., Feld M.S. *Phys. Rev. Lett.*, **72**, 1341 (1994).
31. Niziachristos V., Yodh A.G., Schnall M., Chance B. *Proc. Natl. Acad. Sci. USA*, **97**, 2767 (2000).
32. Intes X., Niziachristos V., Culver J.P., Yodh A.G., Chance B. *Phys. Med. Biol.*, **47** (1), (2002).
33. Culver J.P., Choe R., Holboke M.J., Zubkov L., Durduran T., Slemp A., Niziachristos V., Chance B., Yodh A.G. *Med. Phys.*, **30**, 235 (2003).
34. Zhang Q., Brukilacchio T.J., Li A., Stott J., Chaves T., Hillman E., Wu T., Chorlton M., Rafferty E., Moore R.H., Kopans D.B., Boas D.A. *J. Biomed. Opt.*, **10**, 024024 (2005).
35. Kazantsev I.G., Pickalov V.V. *Signal Processing*, **78**, 117 (1999).
36. Konovalov A.B., Kiselev A.N., Vlasov V.V. *Pattern Recognition and Image Analysis*, **16**, 249 (2006).
37. Nagy J.G., Palmer K., Perrone L. *Numerical Algorithms*, **36**, 73 (2004).
38. Hanke M., Nagy J.G. *Inverse Problems*, **12**, 157 (1996).
39. Ng M.K., Chan R.H., Tang W.-C. *SIAM J. Sci. Comput.*, **21**, 851 (1999).
40. Kaufman L. *IEEE Trans. Med. Imag.*, **12**, 200 (1993).
41. Paige C.C., Saunders M.A. *ACM Trans. Math. Softw.*, **8**, 43 (1982).
42. Bjorck A. *Numerical Methods for Least Squares Problems* (Philadelphia, PA: SIAM, 1996).